The Fluid Mechanics of Carbon Dioxide Sequestration

Herbert E. Huppert[1–3] and Jerome A. Neufeld[4]

[1]Institute of Theoretical Geophysics and Department of Applied Mathematics and Theoretical Physics, University of Cambridge, Cambridge CB3 0WA, United Kingdom; email: heh1@cam.ac.uk

[2]School of Mathematics, University of New South Wales, Kensington NSW 2052, Australia

[3]Faculty of Science, University of Bristol, Bristol BS2 6BB, United Kingdom

[4]BP Institute, Department of Earth Sciences, and Department of Applied Mathematics and Theoretical Physics, University of Cambridge, Cambridge CB3 0EZ, United Kingdom; email: j.neufeld@bpi.cam.ac.uk

Annu. Rev. Fluid Mech. 2014. 46:255–72

First published online as a Review in Advance on September 4, 2013

The *Annual Review of Fluid Mechanics* is online at fluid.annualreviews.org

This article's doi: 10.1146/annurev-fluid-011212-140627

Keywords

gravity currents, residual trapping, convective dissolution, leakage, geomechanics

Abstract

Humans are faced with a potentially disastrous global problem owing to the current emission of 32 gigatonnes of carbon dioxide (CO_2) annually into the atmosphere. A possible way to mitigate the effects is to store CO_2 in large porous reservoirs within the Earth. Fluid mechanics plays a key role in determining both the feasibility and risks involved in this geological sequestration. We review current research efforts looking at the propagation of CO_2 within the subsurface, the possible rates of leakage, the mechanisms that act to stably trap CO_2, and the geomechanical response of the crust to large-scale CO_2 injection. We conclude with an outline for future research.

1. INTRODUCTION

Undeniably, the average global carbon dioxide (CO_2) content of the atmosphere has increased from 315 ppm in 1960, when direct measurements in the atmosphere were first taken by Charles Keeling, to 400 ppm currently (May 2013). The concentration has varied from its lowest (170 ppm) 650,000 years ago to its present maximum. At the moment 32 gigatonnes of CO_2 is released annually into the atmosphere by humans, as identified by its isotopic composition. Closely correlated to this CO_2-concentration measurement, the average global temperature of the atmosphere at the surface of the Earth has varied on many time scales, ranging from approximately 9°C colder than present to 6°C warmer (Lüthi et al. 2008), with large spatial variations at any time. The temperature record is generally much noisier than the CO_2 record and shows an increase over the past 150 years of some 0.8°C, from approximately 14.6 to 15.4°C.

The two major components of the atmosphere—nitrogen and oxygen—have no greenhouse effect, as first shown by Tyndall in the early 1880s, whereas three relatively rare components—water vapor (1.5–2% by volume), CO_2 (0.04%), and methane (2 ppm)—have comparatively large effects, with methane having the largest effect per unit mass, although it deteriorates most rapidly of the three within the atmosphere. (Methane is 70 times more effective per unit mass as a greenhouse gas than CO_2 over the first 20 years, which decreases to 25 times over 100 years. At the moment, 0.6 gigatonnes of methane is vented to the atmosphere, mainly through wetlands and ruminating cows.)

Worldwide, most (85%) of the energy use by humans is generated by the burning of fossil fuels (coal, natural gas, and petroleum); approximately 25% of that is at power stations, and the remainder includes another 20% by industrial processes and 13% by transport. The amount of CO_2 emitted by humans into the atmosphere has increased approximately linearly at the rate of order 1% per year since at least 1980. As first predicted by Tyndall in the late 1850s, further input of CO_2 into the atmosphere will lead to further increases in temperature, with potentially disastrous effects.

What can be done about this global problem, given that the residence time of atmospheric CO_2 is roughly 50 years? The two authors, and many other scientists, are of the opinion that it is unlikely that humans will change their habits and use less energy. Geoengineering (Shepherd et al. 2009)—changing the atmosphere by the introduction of large mirrors in space or the release of sulfur dioxide, both of which reflect sunlight—is a possible solution, but it might lead the Earth into an unpredicted, unknown, and dangerous state. The capture of CO_2 from stationary sources such as power plants and gas-production sites (but not directly from the atmosphere, which is an expensive undertaking) seems an obvious solution. Storage in the many available and large reservoirs of porous rock, kilometers beneath the surface of the Earth, seems a bright possibility. The sequestered CO_2 becomes supercritical (or liquid-like) below a depth of approximately 800 m (dependent on the background temperature gradient) and has a density of approximately 600 kg m^{-3} (in contrast to approximately 2 kg m^{-3} at the surface). Its motion through the reservoir is governed by fluid mechanics, as described in the rest of the article.

The questions addressed here include the following. How far and fast does the CO_2 flow from the release point? Does the CO_2 dissolve into any of the interstitial fluid, often brine, and what happens to this mixture? If there is a leak (through a fracture, a fault, or an old well), how rapidly will the CO_2 escape, and what effect might this have? What are the increases of pressure at the source point and also in the far field?

All these fluid mechanical questions are confronted in the next sections, which present the results of theoretical analyses, laboratory simulations, and field experiments, as illustrated in **Figure 1**.

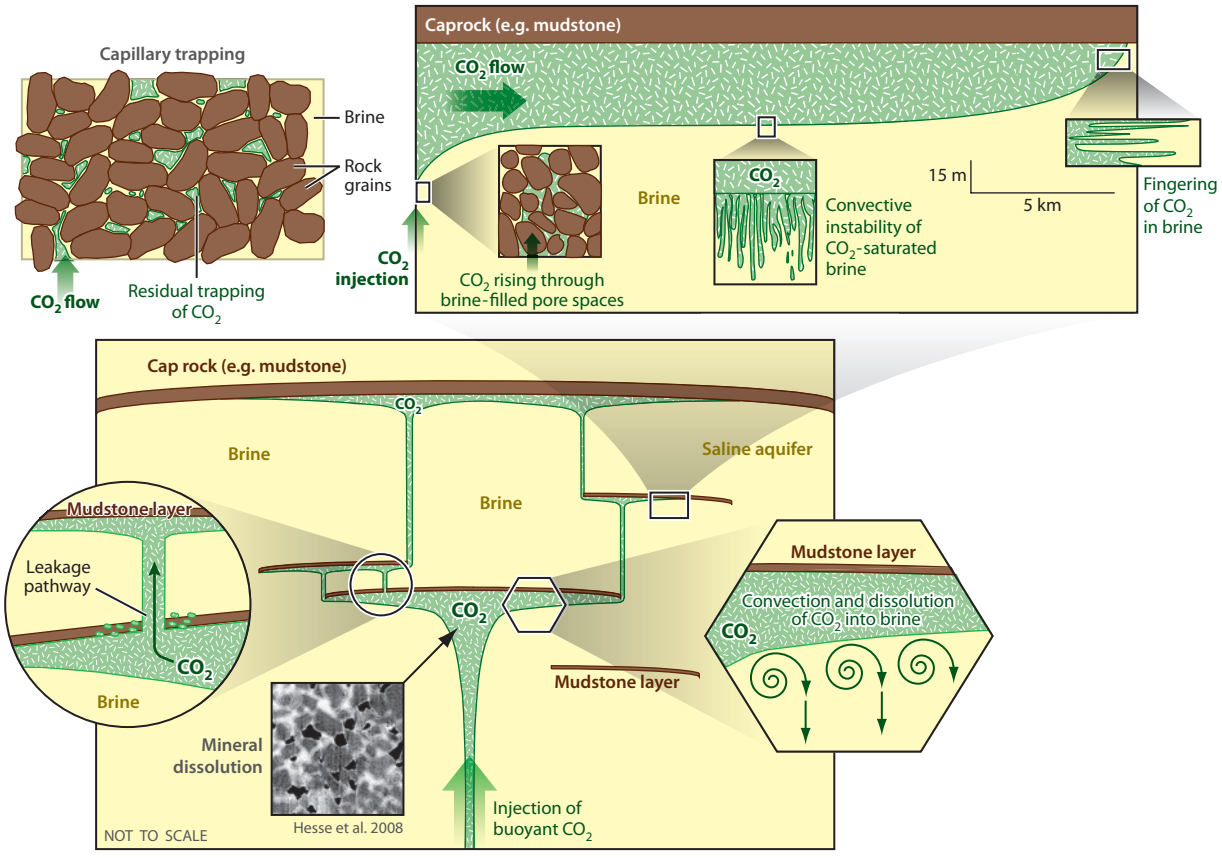

Figure 1

Overview of the fluid dynamics associated with the geological storage of CO_2, including buoyancy-driven spreading, leakage, and residual trapping due to dissolution and capillary trapping.

Possible reservoirs for CO_2 include uneconomical brown coal seams, old oil reservoirs (they have at least displayed the ability to store oil for over millions of years), and saline aquifers in which the largest storage potential is thought to exist. The injection of CO_2 into saline aquifers is typically envisaged at depths between 800 and 3,000 m, where the CO_2 exists in a supercritical state. The flow of CO_2 and ambient brine depends on the relative densities and viscosities of the two fluids, both of which depend on the temperature and pressure (and hence depth) of the aquifer. In addition, the density of ambient brine is a function of its salinity. Nordbotten et al. (2005) surveyed the fluid properties for cold to warm aquifers with surface temperatures between 10 and 20°C, and typical geothermal gradients between 25 and 45°C km^{-1}. For shallow aquifers at depths of approximately 1,000 m, the density of CO_2 may vary due to temperature, from $\rho_c = 266$ to 714 kg m^{-3}, whereas the corresponding density of water, which may depend both on temperature and on salinity, varies from $\rho_w = 998$ to 1,230 kg m^{-3}. In comparison for deep aquifers at depths of approximately 3,000 m, the density of CO_2 varies from $\rho_c = 479$ to 733 kg m^{-3} and the density of brine from $\rho_w = 945$ to 1,202 kg m^{-3}. Correspondingly, the viscosities for CO_2 and water may be in the range $\mu_c = 0.023$–0.0611 mPa·s and $\mu_w = 0.195$–1.58 mPa·s, respectively. Thus, the ratio of densities between CO_2 and water is large and may lie in the range

$\rho_c/\rho_w = 0.22$–0.75, and the viscosities lie within the range $\mu_c/\mu_w = 0.026$–0.22. In addition, under these conditions, CO_2 is partially soluble in water (typically ≈3 wt%). As shown below, both surface tension and dissolution have important implications for the spread and trapping of CO_2. Given such large density differences, the buoyant rise of CO_2 within an aquifer must first be halted by a cap rock, strata with relatively low permeability. Thereafter, the dynamics of spreading is dominated by buoyancy-driven spreading along the cap rock. The implication is that, even if injection is curtailed, CO_2 may continue to spread, continually sampling the cap rock and thereby maintaining the risk of leakage. An important question therefore is over what time and length scales will trapping mechanisms ultimately halt the spreading of buoyant CO_2, thus reducing the risk of potential leakage.

Small pilot studies and large-scale industrial trials, in which CO_2 is injected into a variety of geological settings, are already underway and provide much of the motivation, and a critical test, for the fluid dynamical ideas presented here. Perhaps the most important project is the Sleipner project in the North Sea, owing principally to the wealth of seismic data available to image the spread of the injected CO_2. There, waste CO_2 from an offshore natural gas–production facility has been reinjected since 1996 at a depth of just over 1 km below sea level, and a rate of roughly 1 Mt year^{-1} (megatonnes CO_2 injected per year) since 1996 into the Utsira sandstone, a 200–300-m-thick, highly porous, and permeable reservoir. This wealth of seismic data, acquired in six repeat surveys over 11 years, shows the rise and spreading of the CO_2 plume at nine distinct horizons throughout Utsira (see **Figure 2**) (Bickle et al. 2007, Boait et al. 2012). To leading order, the areal extent at each horizon generally increases linearly in time, a point we return to shortly. Other significant industrial-scale CO_2 storage projects include the In Salah project in the Algerian desert, in which the roughly 0.5 Mt of CO_2 injected per year has resulted in surface deformation that has been mapped using interferometric synthetic aperture radar (InSAR) (see Rucci et al. 2013), and at Weyburn, Canada, where 2–3.5 Mt year^{-1} of CO_2 is currently injected as part of an enhanced oil-recovery project (White et al. 2004).

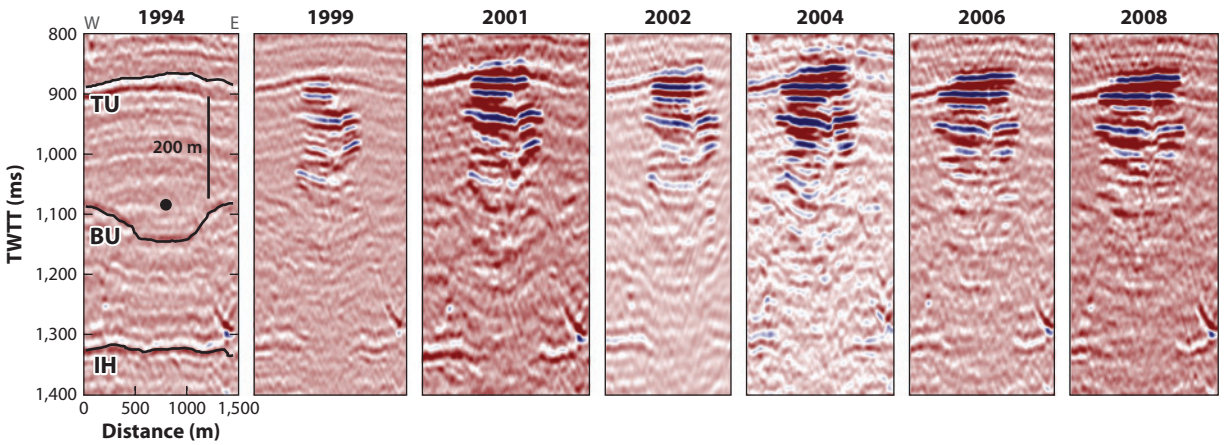

Figure 2

Seismic images showing cross sections of the two-way travel time (TWTT) seismic reflectance amplitude. Clearly shown are the bounding cap rock and base in the preinjection survey (1994) along with the accumulation of CO_2 in subsequent years at a series of nine thin-shale barriers. The black dot is the injection point, TU is the top of the Utsira sandstone (the Nordland shale), BU is the bottom of the Utsira (Hordaland shale), and IH is a lower, intra-Hordaland seismic reflection. Figure adapted from Boait et al. (2012, figure 3).

2. SIMPLE FLOW MODELS

2.1. Single-Phase Models of Buoyant CO_2 Propagation

Confined propagation: the motion of a gravity current in a porous layer of finite thickness influenced by the return flow

Sharp-interface model: model simplification treating the flow of carbon dioxide as separated from ambient brine by a sharp interface

Buoyancy velocity: natural velocity of carbon dioxide, driven by gravity acting on the density difference, $\Delta\rho$, between carbon dioxide and brine in a porous medium with permeability K

The large density contrast between CO_2 and ambient brine, along with the large volumes envisaged being injected, implies that the likely footprint of injected CO_2 will be large. In addition, the flow will be driven principally by a combination of injection pressures, particularly in the near wellbore environment, and buoyancy. In this limit, simple yet informative models have been constructed in which the depth of the current is very much less than its lateral extent. Such porous gravity current models, in which the two phases occupy distinct regions, are sometimes called sharp-interface models and predict the evolution of the depth, $h(x, y, t)$, of the current. Because of the large aspect ratio, flow is mainly lateral, and hence pressure within the current is principally hydrostatic. Flows can then be of two forms. If the current spans the depth of the reservoir, typically near the injection point, the current is confined, and the motion of the ambient fluid plays an important dynamical role. In contrast, when the depth of the current is very much less than that of the reservoir, the ambient fluid plays no dynamical role, and the current is unconfined.

For confined flows in a horizontal aquifer of thickness H, where flow is driven both by the background pressure gradient and by gradients in the local hydrostatic pressure, the evolution of the profile can be found by evaluating the horizontal velocity using Darcy's equation (Bear 1972, Phillips 1991), along with vertical integration of local mass conservation, which leads to

$$\phi\frac{\partial h}{\partial t}+\hat{\mathbf{n}}\cdot\nabla\left(\frac{MQh}{H+(M-1)h}\right)-u_b\nabla\cdot\left[\frac{h(H-h)}{H+h(M-1)}\nabla h\right]=0 \qquad (1)$$

(Hesse et al. 2007, Huppert & Woods 1995, Nordbotten & Celia 2006). Here Q is the input volume flux, $\hat{\mathbf{n}}$ is the unit normal in the direction of the pressure-driven flow (e.g., $\hat{\mathbf{x}}$ in linear coordinates and $\hat{\mathbf{r}}$ in radial coordinates), $u_b = K\Delta\rho g/\mu_c$ is the natural buoyancy velocity of CO_2 in water, K is the permeability of the medium (which in general can be an anisotropic and spatially varying tensor), $\Delta\rho = \rho_w - \rho_c$ is the density difference between water and CO_2, $M = \mu_c/\mu_w$ is the ratio of viscosities (CO_2/water) known as the mobility ratio, and ϕ is the porosity. The problem is solved subject to a condition on the mass flux at the origin, or equivalently subject to a statement of global mass conservation, written as

$$V(t)=\int_D \phi h(x,t)dxdy, \qquad (2)$$

where D is the horizontal area (2D region) occupied by the current.

Further from the injection point, where $h \ll H$, the second term in Equation 1 becomes negligible, and the third term becomes independent of H and M. In this limit, the current becomes unconfined, and the flow of ambient fluid along with the mobility ratio can be neglected, as described elegantly for the spreading of a constant volume in two dimensions (Hesse et al. 2007). When the current spreads radially from a source with constant input flux Q, Equations 1 and 2 reduce to

$$\phi\frac{\partial h}{\partial t}-u_b\nabla\cdot(h\nabla h)=0, \qquad (3a)$$

$$V(t)=Qt=2\pi\phi\int_0^{r_N} h(r,t)rdr, \qquad (3b)$$

where $r_N(t)$ is the radial extent of the current. This unconfined model was initially derived to describe the spreading of CO_2 at the Sleipner project as imaged in successive seismic surveys (Lyle et al. 2005). There are two main results of the study. First, after a relatively short time, the

behavior is well described by a similarity solution in which the radial extent is given by

$$r_N(t) = \eta_N (u_b Q/\phi^2)^{1/4} t^{1/2}, \tag{4}$$

where $\eta_N \simeq 1.17$. The second result is that, except close to the source, the thickness of the current, $h(r, t)$, is to a good approximation linear in the radial coordinate and is given by

$$h(r,t) = \frac{\eta_N^2}{2}(Q/u_b)^{1/2}[1 - \eta_N^{-1}(u_b Q/\phi^2)^{-1/4} r t^{-1/2}]. \tag{5}$$

A linear relationship between the areal extent, which is directly proportional to r^2, and t was found for much of the initial data from Sleipner, in good agreement with the theory (Bickle et al. 2007, Boait et al. 2012). At later times, the behavior at each layer varies, with some increasing linearly in area, while others remain constant or decrease in areal extent. This may result from any number of factors, including vertical migration through the thin, relatively impermeable layers as a uniform flow or through discrete fractures and dissolution at the CO_2-water interface.

When buoyant gravity currents spread along a slope at angle θ to the horizontal, the upslope component of gravity must be included, so that Equation 3a is replaced by

$$\phi \frac{\partial h}{\partial t} - u_b \nabla \cdot [\cos\theta h \nabla h - \sin\theta h \hat{\mathbf{x}}] = 0, \tag{6}$$

where here $\hat{\mathbf{x}}$ is the unit vector in the along-slope direction. For a buoyant current whose volume can be parameterized as $V(t) = q t^{\alpha}$, the spreading of the current is axisymmetric for times much less than $t^\star = (q\phi^2/u_b^3 \tan\theta)^{1/(3-\alpha)}$. At longer times, the current ceases to progress downslope, and the upslope extent increases as $x_u \propto u_b t$ (Vella & Huppert 2006).

Effects of a more general topographic variation were investigated by Pegler et al. (2013), who considered the injection from a point source of fluid into a domain bounded by, in the most general case, topographical variations whose displacement from the horizontal is described by elliptical contours

$$d(x, y) = a|x|^m + b|y|^n, \tag{7}$$

where x and y are mutually orthogonal axes in the horizontal, and m and n can take any positive value [either m or n equaling zero represents two-dimensional topography, independent of one of the coordinates (Golding & Huppert 2010), whereas $m = n = 2$ and $a = b$ represent parabolic, axisymmetric topography]. They found that for a two-dimensional flow ($m = 0$), the behavior of the flow at a constant flux depends significantly on the value of n. For $n > 1/2$, the flow evolves from an early time, self-similar form (dependent on both space and time) increasing in length with time like $t^{2/3}$, which transitioned into a flow controlled only by the geometry of the boundary, and having a horizontal free surface. For $n < 1/2$, the transition between these two flow regimes is reversed with a topographically controlled flow, with an almost horizontal free surface, being replaced by a similarity solution insensitive to the geometrical variations at later times. For axisymmetric flows ($m = n = 2$), the transition with time is always from a similarity solution to one with a nearly horizontal free surface. Careful analysis of the data from Sleipner shows a roughly elliptical outline for the sequestered CO_2 with nearly constant aspect ratio for all times. An explanation other than topographic variations, possibly spatial porosity and permeability variations in the porous reservoir, will be needed and is being sought.

2.2. Multiphase Models of Buoyant CO_2 Propagation

Single-phase, or sharp-interface, models provide considerable insight into the dynamics of spreading CO_2 but do not resolve the influence of surface tension acting between the phases. When surface tension acts between CO_2 and brine within the varied pore geometry of the reservoir,

each phase occupies only a fraction of the pore space, thus resulting in differing local saturations of the two phases. This has two important implications for the flow of CO_2. First, the effective pore size is reduced as brine continues to occupy some of the rock pores. Second, the resistance to flow, as measured by the intrinsic permeability of the rock, differs when both phases are present. Multiphase models of propagating CO_2 must therefore account for variations in both the effective porosity, or saturation, and the relative permeability of the two phases. Modeling begins with an empirical relationship relating the capillary pressure between the phases to the local saturation, accounting for both the wetting properties of the rock and the pore-size distribution. In the limit of nearly horizontal flow discussed earlier for simple models of propagation, the pressure within both phases is approximately hydrostatic, and the difference in the pressure between the phases is given by an empirical capillary pressure that therefore determines the saturation, or local effective porosity, of CO_2. Propagation is then determined by the relative permeability of each phase, which in turn depends empirically on the local saturation.

Multiphase model: model incorporating the effect of surface tension acting between the two fluids within the convoluted confines of the pore space

Residual, or capillary, trapping: confinement of the carbon dioxide within the pore spaces due to the action of surface tension between phases

The complexity of the formulation is increased considerably, but the vertically integrated formulations for confined (Gasda et al. 2009) and unconfined aquifers (Golding et al. 2011, 2013) find evolution equations for the propagating CO_2 that are remarkably similar to Equations 1 and 3, respectively. For example, these studies found that for axisymmetric currents spreading in an unconfined aquifer, the rate of propagation is highly insensitive to capillary effects, while the profile and thickness of the current can be dramatically altered, and depends on the strength of capillary forces, the pore-size distribution of the porous rock, and the depth-averaged relative permeability of the two phases. The effect of capillary forces can be described by a Bond number, $B = \Delta\rho g L_H / p_e$, where p_e is the capillary pressure necessary for CO_2 to invade the largest pores, and $L_H = (Q/u_b)^{1/2}$ is the natural, time-independent length scale in an unconfined aquifer. In general, capillary forces tend to broaden or thicken the current, an outcome which can be understood by noting that the reduced saturation concomitant with the increased effectiveness of capillary forces results in a reduced effective porosity and permeability as seen by the intruding CO_2.

These hybrid models effectively bridge the gap between simple, yet physically insightful, models of porous gravity currents and full-scale numerical simulations of multiphase propagation. The utility of these models is both in their provision of robust predictions of the implications of capillary effects on large-scale propagation and in their ability to implicitly resolve the vertical structure of saturation, thus reducing the computational costs of highly resolved aquifer-scale numerical models. Finally, we note that the retention of CO_2 within the pore space through the action of capillary processes, resulting in residual trapping as discussed in more detail below, is a process that depends sensitively on the local saturation. Hence, large-scale multiphase gravity current models, which implicitly resolve the vertical gravity-capillary balance, have an important role in our understanding of how CO_2 propagates, and is ultimately trapped, within the subsurface.

3. CONTAINMENT AND LEAKAGE OF CO_2

The current rate of anthropogenic emissions of CO_2 requires technological solutions on a grand scale. This implies that for carbon sequestration schemes to play a significant role, vast subsurface reservoirs must be found. As seen above, buoyancy-driven propagation of sequestered CO_2 may lead to a large area of the bounding cap rock being sampled by the spreading plume, with a concomitant risk of leakage or vertical migration throughout the formation. Two modes of leakage have been studied previously: uniform leakage through lower-permeability layers and discrete leakage through relatively high-permeability pathways in an otherwise impermeable cap rock. Some motivation for both these modes of leakage can be found, for instance, in seismic images of the spreading of injected CO_2 at Sleipner, in the Utsira formation under the North Sea. There,

time-lapse images show the migration of buoyant CO_2 through nine distinct, thin mudstone layers in a manner that is consistent with a combination of both distributed upwelling and upwelling through a series of discrete, high-permeability pathways.

In nearly all potential sequestration reservoirs, the natural layering of the host rock can lead to variations in the pore geometry and porosity, both potentially leading to variations, by several orders of magnitude, in permeability. As a result, the variation in permeability between primary storage and low-permeability cap rock can be large, and the approximation that pressure within the buoyant CO_2 plume is nearly hydrostatic can still be satisfied in the presence of significant leakage (Pritchard et al. 2001). Most models of leakage therefore assume that the difference in pressure between the plume and the ambient drives fluid flow. These ideas were first formulated, and experimentally tested, for a viscous current overriding a deep porous medium by Acton et al. (2001) and for variations in permeability by Pritchard et al. (2001). The leakage velocity in this case is given by

$$w_l = -\frac{k_b}{\mu_c}\frac{\Delta\rho g h}{b} = -u_b\frac{k_b}{k}\frac{h}{b}, \tag{8}$$

where w_l is the leakage velocity, k_b the permeability of the bounding cap rock, $\Delta\rho$ the difference in densities between ambient and injected fluids, h the depth of the CO_2 plume, and b the thickness of the low-permeability cap rock. The addition of a leakage term changes the evolution equation for the CO_2 plume at each layer (Equation 3a) to

$$\phi\frac{\partial h}{\partial t} - u_b\nabla\cdot(h\nabla h) = w_l \tag{9}$$

and importantly results in the possibility of an ultimate steady state, in which the injected volume equals that uniformly leaking through the low-permeability layer. Pritchard et al. (2001) examined a suite of possibilities and found analytical expressions for the steady-state profile and maximal extent of the current in two dimensions,

$$h(x) = \frac{\lambda}{6}\left[x - \left(\frac{18}{\lambda^2}\right)^{1/3}\right]^2 \quad \text{and} \quad x_n(t\to\infty) = \left(\frac{18}{\lambda^2}\right)^{1/3}, \tag{10}$$

where lengths are scaled by $\phi Q/u_b$ and $\lambda = (k_b/k)(\phi Q/u_b)/b$. A similar balance exists for radially spreading currents, with a solution that must be solved numerically. These ideas have been extended to a geometry more reminiscent of the layered Sleipner formation by Neufeld & Huppert (2009), who considered the lateral propagation and vertical seepage of CO_2 through a layered porous medium. Their model assumed that fluid remained continuously connected as it traversed through the porous medium and hence formulated a drainage law as

$$w_l = -u_b\frac{k_b}{k}\left[1 + \frac{h(r,t)}{l(r,t)}\right], \tag{11}$$

where $l(r, t)$ is the extent to which the current has drained past the low-permeability layer. This additional assumption, that fluid remains connected, results in an initial maximal extent at each layer followed by a gradual retreat to the final steady-state radius of the current, r_N, given by

$$r_N = \left(\frac{Q}{\pi u_b}\right)^{1/2}. \tag{12}$$

A limitation of these drainage models is their neglect of capillary forces. Although capillary forces act throughout the body of the CO_2 plume, they are especially important at the interface between media of differing pore sizes or geometry, which determines the permeability. In this case, a finite capillary entry pressure p_c must be overcome by the hydrostatic pressure in the CO_2 current for

leakage to occur. This leads to a critical capillary height, $h_c = p_c/\Delta\rho g$, as defined by Woods & Farcas (2009), below which no leakage occurs and above which fluid can migrate through the low-permeability layer.

Within geologically complex formations, and in reservoirs already punctured by exploration and production wells, leakage from discrete fractures, faults, or unused boreholes is a distinct possibility. A range of potential geometries has been explored in confined (Nordbotten & Celia 2006) and unconfined aquifers (Neufeld et al. 2009, 2011; Pritchard 2007; Vella et al. 2011). For leakage from unconfined currents, an instantaneous efficiency of storage can be defined as

$$E_s = (Q - Q_l)/Q, \tag{13}$$

Efficiency of storage: an instantaneous measure of the quantity of carbon dioxide stored; equal to the difference between the injection rate Q and leakage rate Q_l normalized by the injection rate

equal to the difference between the rate at which fluid is injected, Q, and the leakage rate, Q_l, normalized by the injection rate. Leakage is driven by the pressure drop across the leakage pathway, which in unconfined aquifers may be modeled as the difference between the pressure within the current and the ambient hydrostatic pressure. In addition, a general feature of horizontal propagation during the injection phase is the concomitant growth of the depth of the current at all points along its path. The consequence is that the pressure difference driving leakage from the current increases with time, hence decreasing the efficiency of storage. The precise details of the decrease in the efficiency of storage depend intimately on the geometry of the reservoir and of the leakage pathway. For example, in the asymptotic limit of large times, a model of planar flow from a line of injection wells to a parallel linear fracture predicts $E_s \propto t^{-1/2}$, whereas for radial flow from an injection well to a localized point of leakage, $E_s \propto 1/\ln(t)$, or to a planar fault or fracture, $E_s \propto t^{-2/5}$. In each case, the particulars of the aquifer and leakage pathway (e.g., permeabilities, porosities, distances) can be quantitatively captured by the prefactor and agree well with full solutions of the governing equations and with laboratory experiments in the planar situation (the only geometry for which experiments have been conducted). However, the solutions share the common feature that, in all cases, the efficiency of storage $E_s \to 0$ as $t \to \infty$. This contrasts with leakage from a current within an inclined aquifer, where the depth of the current, and hence the pressure difference driving leakage, is limited by the along-slope component of gravity. Thus, the efficiency of storage is nonzero, $E_s(t \to \infty) =$ constant, at long times (Zimoch et al. 2011).

These studies highlight the role of reservoir and leakage pathway properties along with the geometry of the reservoir. In particular, these relatively simple models of leakage from confined and unconfined reservoirs highlight the central role buoyancy-driven flow in the reservoir plays in determining leakage rates, even for the most permeable fractures. However, many crucial questions remain. CO_2 may leak gradually into overlying strata, where it could subsequently become trapped, or it may rise through relatively unconstrained regions (fractures or uncapped wells), where the exsolution of gaseous CO_2 could drive much more rapid leakage. An intriguing and informative natural example of such activity is the dynamics of Crystal Geyser in Green River, Utah (Bickle 2009), where CO_2 derived from magmatic sources escapes in the form of a periodic, cold-water geyser.

4. TRAPPING MECHANISMS

The aim of CO_2 sequestration is the long-term, or indeed permanent, burial of CO_2 within the subsurface. Upon injection, the initial and primary trapping, or containment, of this buoyant fluid is accomplished by intervening low-permeability cap rock (**Figure 1**). The spreading of CO_2, driven either by the pressures of injection or by its own buoyancy (as described in Section 2), implies that the potential risk of buoyant fluid migrating to a leakage pathway through the cap rock may increase both during and after injection.

This possibility of leakage has spurred significant research into a range of new fluid mechanical processes that ultimately play an important role in trapping buoyant CO_2 permanently. First, the

dissolution of CO_2 into ambient brine occurs from the onset of injection through post-injection migration. Dissolution occurs when the CO_2 contacts ambient brine or water and may thus be greatly enhanced by mixing due to dispersion and flow through heterogeneities within the host rock. Intriguingly, variations in CO_2 concentration within the brine may also lead to convection, a process that could greatly enhance the flux of dissolved CO_2 in some aquifers. Second, capillary forces between injected CO_2 and brine may act to trap CO_2 as small ganglia within the rock, a process known as residual, or capillary, trapping. This process occurs at retreating CO_2-brine interfaces and thus is of primary importance in the post-injection phase. Finally, on much longer time scales, CO_2 may precipitate as carbonates, perhaps the ultimate form of stable trapping, although this is not a process we consider here.

Convective dissolution: convective motion driven by the density difference between carbon dioxide–saturated and unsaturated brine in which the dissolution of immiscible, supercritical carbon dioxide is the source of carbon dioxide–saturated water

4.1. Convective Dissolution

A promising avenue for the stable trapping of CO_2 is through the dissolution of buoyant CO_2 in the ambient brine, which is ultimately accomplished through the mixing of injected (immiscible) CO_2 with ambient brine. The dissolution of CO_2 into brine therefore removes buoyant CO_2 from the system, thus reducing the risks of vertical migration or leakage. Perhaps most intriguingly, from a fluid dynamical perspective, the density of brine is known to increase with increasing CO_2 concentrations up to $C \simeq 3$ wt% at typical reservoir temperatures and pressures (the point at which water becomes fully CO_2 saturated). Thus, the dissolution of CO_2 into brine gives rise to density differences within the brine driven by gradients in CO_2 concentration, and these density gradients may in turn drive further convection of CO_2-saturated brine. Dissolution-driven convection, as with thermally driven convection, can dramatically enhance the rate of CO_2 dissolution and thus has an important role in stabilizing sequestered CO_2 (Ennis-King & Paterson 2005).

A typical scenario, depicted in **Figure 1**, is of the dissolution of CO_2 from the base of buoyant currents propagating within saline aquifers. Motivated by this scenario, much early work in this area has focused on the long-outstanding question of the onset and evolution of convection from a quiescent or stagnant pool of CO_2, as might be found, postinjection, in an anticlinal trap.

In general, porous convection in a saline aquifer can be characterized by a porous Rayleigh number,

$$Ra = \frac{g\Delta\rho_c K H}{\mu_W \phi D}, \tag{14}$$

where $\Delta\rho_c$ is the density difference between unsaturated and CO_2-saturated brine, which drives the convection; D is the diffusivity of CO_2 in water; and H is the full depth of the aquifer. The transient onset of convection in the brine into a deep reservoir is driven by the dissolution of CO_2 from the stationary contact between supercritical CO_2 and brine. The resulting diffusive wedge of CO_2-saturated, and therefore dense, water grows diffusively with a length scale, $\delta(t) \propto \sqrt{Dt}$. Convection ensues when the Rayleigh number characteristic of the boundary layer exceeds a critical value, $Ra_{\mathrm{bl}} = Ra\delta/H \geq Ra_c$. Hence, from an initially quiescent state with a sharp interface between CO_2 and brine, convection is expected after a critical time

$$10\,\mathrm{days} < t_c = c\,\frac{H^2}{D}\left(\frac{Ra_c}{Ra}\right)^2 < 2{,}000\,\mathrm{years}, \tag{15}$$

for a range of possible permeabilities from $1mD$ to $3D$ (1×10^{-15} to 3×10^{-12} m^2), where $c \simeq 0.1$, taking $Ra_c = 4\pi^2$ (Riaz et al. 2006, Slim & Ramakrishnan 2010). The precise nature of the onset of convection in porous media from a transient base state has been the subject of intense study. However, it is likely that at the early stages of injection into even moderately heterogeneous reservoirs, dissolution is dominated by mixing induced by forced or buoyancy-driven flow through

the porous medium. Thus, in reservoirs in which convection is expected (i.e., with $Ra > Ra_c$), the onset of convection is likely to be driven by mechanical mixing of the fluids, rather than the diffusive onset discussed above.

The range and scope of aquifers considered for injection imply that the Rayleigh number can span a large range. For example, the Utsira sandstone, in which approximately 1 Mt year^{-1} of CO_2 is currently being injected under the North Sea, is a relatively deep and porous aquifer with a correspondingly large Rayleigh number, $Ra \simeq 10^4$ (for an intershale thickness $H \simeq 20$ m). In such cases, convection is expected to be vigorous, and this motivates the study of the character of high–Rayleigh number convection.

The transient convection of CO_2-saturated water from the immiscible (supercritical) CO_2-water interface into a deep aquifer is governed by the same physical balances that govern thermal and composition porous convection in other geophysical systems. Therefore, whereas dissolution-driven convection of CO_2-saturated waters occurs from the upper boundary alone, so-called one-sided convection, convection between a cold upper boundary and a hot lower boundary, so-called two-sided convection, contains many of the same physical balances. Importantly, the case of two-sided convection can be studied in a statistical steady state and therefore provides a more penetrating test of the small-scale dynamics driving the transient one-sided convection typical of dissolved CO_2.

For two-sided convection, it is now well established that the onset of convection occurs at $Ra_c = 4\pi^2$ (Lapwood 1948) as a series of rolls with wave number $k \sim \pi$ (Neild & Bejan 2006). In two dimensions, these rolls become unstable to a series of dripping instabilities (Graham & Steen 1994), and at $Ra \geq 1{,}250$ the transition to a high–Rayleigh number regime is characterized by large, long-lived vertical plumes (see **Figure 3**) (Backhaus et al. 2011, Hewitt et al. 2012, Neufeld et al. 2010). Similar localized high–Rayleigh number plumes have also been found in fully three-dimensional numerical simulations (Pau et al. 2010) and in field measurements of convection in a

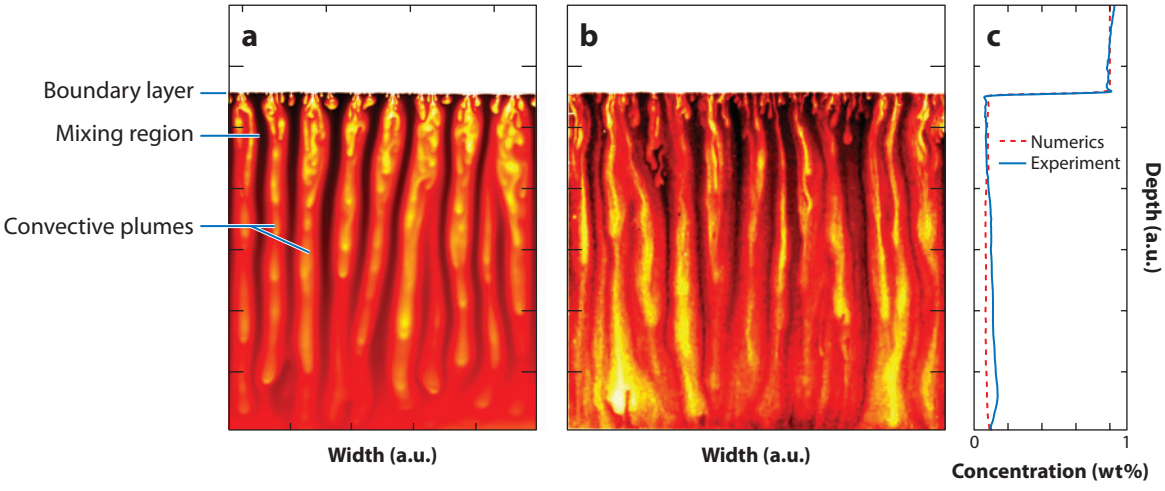

Figure 3

Images of (*a*) numerical and (*b*) analog experiments of high–Rayleigh number convective dissolution. Convection within the interior is dominated by a series of long-lived vertical plumes, fed by proto-plumes that form from an instability of the thin boundary layer and merge within the mixing region. After an initial transient, the horizontally averaged concentration, shown in panel *c* for numerics (*dashed*) and experiment (*solid*), is effectively uniform in the vertical direction and provides the basis for a simple reduced model of convection. Figure modified from Hewitt et al. (2013).

saline aquifer driven by surface evaporation (Stevens et al. 2009). This variety of spatial convective structures is important when considering the numerical simulation of convection in large aquifers. The diffusive boundary length scale, which is the smallest length scale that must be resolved, is of order $\delta \sim H/Ra$, which for Sleipner is 1–10 mm. It is therefore impractical to consider the full numerical simulation of convective dissolution within any storage reservoir, whose lateral scale may measure 100 to many thousands of meters. Instead, of critical importance is the behavior of the convective flux, F_c, which is the macroscale (or upscaled) measure of the efficiency of convection in removing buoyant, supercritical CO_2 from the propagating plume.

Again, physical insight can be gained by appealing to results from two-sided thermal convection, in which a statistically steady convective flux can be found. The Nusselt number,

$$Nu = \frac{F_c}{\phi D \Delta C / H},$$

is the nondimensional measure of the convective flux, F_c, made nondimensional by the effective diffusive flux across the domain. The diffusive flux can itself be written in terms of the concentration difference, ΔC, between fully CO_2-saturated water and unsaturated ambient waters, the porosity ϕ, the diffusivity of CO_2 in water D, and the depth of the aquifer H. For aquifers in which $Ra < Ra_c$, no convection is present, and dissolution is driven solely by the diffusion of CO_2 in brine; hence $Nu = 1$. For $Ra > Ra_c$, the fluid is unstable to convective motion, and the time-averaged nondimensional flux $Nu = Ra/40 \cong Ra/Ra_c$ (Elder 1967). Finally, at much larger Rayleigh numbers, $Ra \gtrsim 1,250$, a classical argument from fluid convection (Howard 1964) suggests that the nondimensional convective flux is linearly proportional to the Rayleigh number,

$$Nu = \frac{F_c}{\phi D \Delta C / H} = cRa = c\frac{g \Delta \rho k H}{\phi D \nu}. \tag{16}$$

Indeed, although there has been some debate around anomalous exponents, with $Nu \propto Ra^n$ for $0.8 < n < 0.9$, from both numerical (Otero et al. 2004) and experimental studies (Backhaus et al. 2011, Neufeld et al. 2010), careful numerical studies of two-sided convection up to $Ra = 4 \times 10^4$ indicate that the ultimate linear regime, $Nu \propto Ra$, is indeed attained asymptotically (Hewitt et al. 2012).

The structure of convection in this high–Reynolds number regime consists of a thin diffusive boundary layer of thickness $\delta \sim Ra^{-1}$, which becomes unstable to proto-plumes that propagate and merge within a mixing region. The merger of these proto-plumes within the mixing region produces the long-lived convective plumes that visually dominate the structure of convection. The structure of these plume is that of a heat exchanger, where

$$C(x, z) = \hat{C}\cos(kx) - \frac{k^2}{Ra} z,\ w(x) = (\hat{C})\cos(kx),\ u = 0. \tag{17}$$

Intriguingly, as the Rayleigh number is increased, the planform of fingered convection becomes increasingly monochromatic and appears to attain an asymptotic scaling $k \propto Ra^{0.4}$, which is, as yet, unexplained (Hewitt et al. 2012).

These results, both classical and new, from statistically steady two-sided thermal convection inform our understanding of convection driven by the dissolution of CO_2 at an upper contact between immiscible and buoyant, supercritical CO_2 and water. While exhibiting many features of statistically steady two-sided convection, convective dissolution from the CO_2-water contact at the top of a closed aquifer brings further rich behavior. As discussed previously, the time scale for the onset of convection indicated by several linear stability analyses of the transient base state may be long (years) but in practice will undoubtedly be significantly shortened by mixing during injection of supercritical CO_2. Once the initial fingers of CO_2-saturated water form at the upper

interface, experimental and numerical studies show that the convective flux is constant while these convective fingers descend to the base of the aquifer. These downwelling fingers of CO_2-saturated brine are balanced by relatively fresh upwelling fingers (**Figure 3**). In a laterally confined or closed aquifer, the constant convective flux regime persists until the CO_2 concentration in the ambient brine begins to increase. The end of the constant convective flux regime is tied to the time when the concentration of upwelling fingers at the CO_2-brine interface begins to increase. Thereafter, the system enters a convective shutdown regime, characterized by a nearly uniform concentration field. In the shutdown regime, relatively straightforward box models can be constructed of the evolution of the convective flux and interior concentration using an adaptation of the high–Rayleigh number $Nu = \alpha Ra$ scaling, now with an evolving mean concentration difference $\Delta C(t)$ (Hewitt et al. 2013). For example, for convection in a closed domain, the average interior concentration ($\overline{C}$) scales as

$$\frac{(\overline{C}) - C_{\max}}{C_{\max} - C_0} = -[1 + \alpha(t - t_0)]^{-1}, \tag{18}$$

where $C_{\max}$ is the maximum CO_2 saturation in brine, C_0 is the initial CO_2 concentration, and t_0 is the onset time of the shutdown regime. Correspondingly, the nondimensional convective flux decays as the average saturation within the reservoir increases,

$$Nu = \alpha Ra_0 \left[1 + \alpha\,(t - t_0)\right]^{-2}, \tag{19}$$

where Ra_0 is the Rayleigh number of the initially unsaturated aquifer. For a permeable reservoir such as the Utsira formation of the Sleipner project, the time scale for shutdown is approximately 0.6 years so that the solute flux from convection will be half in 20 years and one-tenth its original value in 75 years (Hewitt et al. 2013).

Finally, it is clear that the ideas summarized here on convection driven by the dissolution of CO_2 in brine may play an important role in reducing the volume of buoyant CO_2 over time. Simple models incorporating the loss of buoyant CO_2 due to convection from migrating buoyant plumes have already been considered (Pritchard et al. 2001, MacMinn et al. 2012, MacMinn & Juanes 2013) and illustrate clearly that convective dissolution may limit the maximum extent of buoyant CO_2 plumes. The results of Pritchard et al. (2001) discussed above (Equations 9 and 10) can immediately be applied to the propagation of a buoyant CO_2 current with convective loss of CO_2 through convective dissolution of strength w_1. Analog laboratory experiments conducted by MacMinn et al. (2012) showed that the buildup of ambient concentration can significantly reduce the effectiveness of convection, with the result that mobile, undissolved CO_2 remained within their model system for far longer. MacMinn & Juanes (2013) extended the results of Pritchard et al. (2001) to the case of sloping aquifers.

Convective dissolution is therefore an important trapping mechanism whose magnitude and form have already spurred new and innovative research in the convection of fluids in porous media. New studies, exploring the shutdown of convection as CO_2 concentrations increase within the brine and of the mixing of CO_2 induced by injection and migration, will undoubtedly bring new and relevant fluid dynamical ideas to bear on this intriguing process.

4.2. Residual Trapping

Surface tension acting between CO_2 and ambient brine may also act to immobilize the buoyant CO_2 through capillary, or residual, trapping. Capillary trapping, viewed at the scale of the CO_2 plume, occurs when residual CO_2 remains within the rock at a receding CO_2 interface and is the large-scale expression of small-scale trapping of CO_2 ganglia within the pore spaces of the host rock. The multiphase nature of the spreading plume, as discussed in Section 2.2, has been

modeled using a variety of techniques. These approaches each seek to capture, in varying degrees of approximation, the nontrivial saturation distribution of supercritical CO_2 and water within the host rock.

Geomechanical response: change in the rock structure, such as deformation and fracture, due to the input of carbon dioxide

A simple parameterization of the residual trapping of pore fluids, used previously to calculate the spread of a groundwater mound, models the spreading of a mound of uniform saturation (Kochina et al. 1983). As the current recedes, a constant proportion, or residual saturation S_r, of fluid is left behind, and thus the volume of mobile fluid steadily decreases over time. The evolution of both the volume and profile of the mobile phase can still be described by a similarity solution, although of the second type, in which the extent of the current $x_N(t) \propto t^{\beta}$, where β must be found as the solution to a nonlinear eigenvalue problem. Thus a constant volume of CO_2 spreading under a horizontal cap rock will spread indefinitely, although its rate of spreading will slow with time and will depend on the magnitude of residual trapping.

This initial study was extended by Hesse et al. (2008), who considered the spreading of a two-dimensional, confined CO_2 plume along a sloping cap rock. Unlike the horizontal current, the action of gravity in the direction of propagation continues to drive fluid motion upslope. The along-slope component of gravity results in a finite current depth at all times and, somewhat paradoxically, thus results in a finite ultimate extent in direct contrast to the horizontal case. This result arises as the current now contacts, at every stage, a larger volume of the porous rock.

The residual trapping of fluid within porous rock is one of the most effective methods for stably trapping CO_2 after injection, but quantitative predictions rely on the upscaling of capillary effects within the porous matrix to effectively predict both the area of the reservoir that is contacted and the quantity of CO_2 that is left behind. Both the contact area and the efficiency of trapping are ongoing areas of research needing critical input from experiments (both laboratory and field) to constrain and inform capillary trapping rates.

5. GEOMECHANICS

Reducing the impact of anthropogenic emissions through subsurface CO_2 sequestration will require very large volumes of fluid to be stored within the subsurface. A critical component of that injection is the geomechanical response of reservoirs to the injected CO_2. Recent work (Zoback & Gorelick 2013) has argued that injection, at the scales necessary to reduce anthropogenic CO_2 emissions, will inevitably trigger moderate seismicity in regions of the crust that are critically stressed. This then raises key fluid dynamical questions: What is the pressure field associated with large-scale injection of CO_2 as a function of reservoir properties and geometry? How do we best monitor and control the reservoir pressures? If seismicity is induced, is leakage likely, and if so, what are the spatial distribution and magnitude of that leakage?

The coupling between fluid dynamics and the geomechanical response of the reservoir is perhaps best exemplified by InSAR data from central Algeria, which clearly show an uplift of the desert floor around three injection wells of approximately 1.5 cm from July 2004 through May 2008 (see **Figure 4**). The pattern of uplift, and its temporal evolution, illustrates the possibility, at least in this location, of low-cost, remote monitoring of both the fluid flow and geomechanical response of an active CO_2 storage site.

6. CONCLUSIONS

New fluid mechanics has an exciting and important role to play in the societally significant process of CO_2 storage. Industrial plans to store billion of tonnes of supercritical CO_2 could, and should, be brought on stream in the next decade. How far and fast the CO_2 spreads through a porous

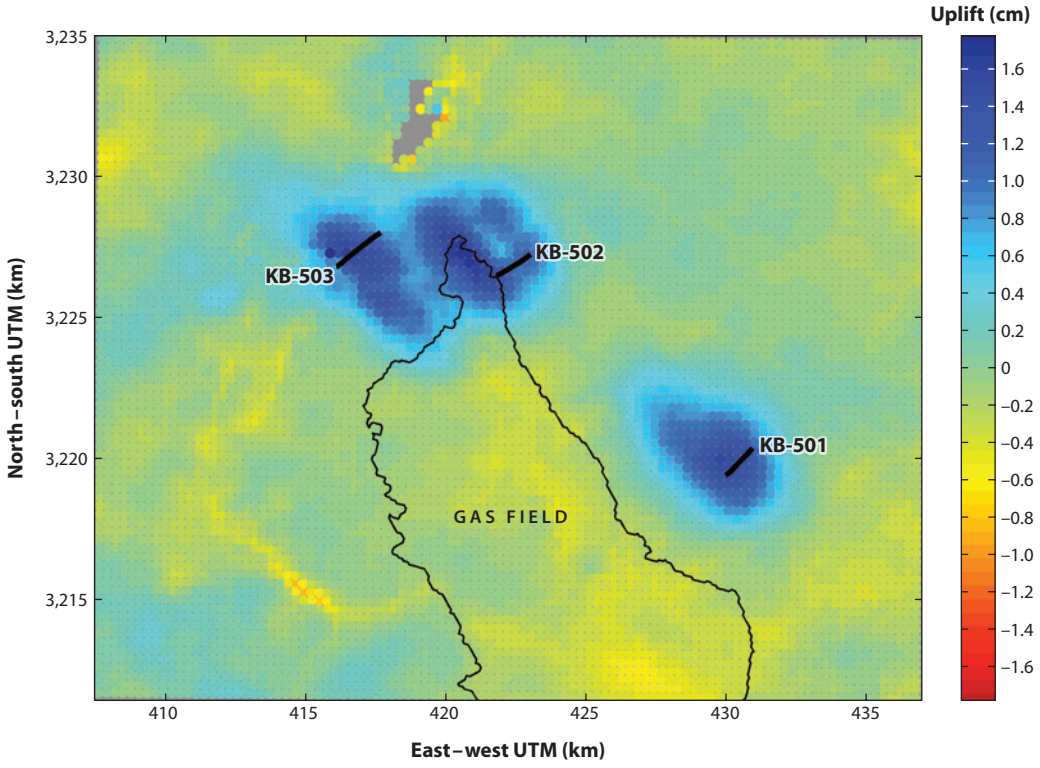

Figure 4

Vertical uplift due to CO_2 injection in three wells at the In Salah CO_2 sequestration project in central Algeria, showing uplift in centimeters as a function of distance north-south and east-west (UTM). Figure adapted from Rucci et al. (2013, figure 11a).

reservoir of spatially varying porosity and permeability need further investigation, although useful and penetrating first attempts have been successfully conducted, as outlined in part in this review.

This review has brought out the different between sharp-interface models, wherein the two fluids—intruding and ambient—are totally separated by an interface, and two-phase models, wherein, owing to surface tension effects, the two fluids coexist within the same pore space. We have also described some effects due to a confining boundary and compared these when the flow is unconfined and effectively takes place in a semi-infinite half space. The different effects of flows on slopes and along horizontal boundaries were outlined as well. The rates and manner of leakage addressed above are important to constrain so that a safe and efficient system of sequestration can be implemented but also so that damaging problems that could greatly diminish public acceptance are avoided.

In contrast, the ambient brine is slightly soluble in the intruding CO_2 to form a mixture that is more dense than either of the end members and therefore sinks to the bottom of the containing reservoir, and the input is hence no longer subject to the possibility of leakage. The dissolution rates are such that at Sleipner, at the moment, of order 10% of the input volume is safely stored every year. This means that if the input was turned off after, for example, 10 years of operation, using linear extrapolation to obtain order-of-magnitude estimates, the input would have been completely mixed and gravitationally trapped after 100 years. Fluid dynamics therefore plays a

central role in determining the risks and future viability of CO_2 sequestration and continues to be an exciting area to apply new physical and fluid dynamical ideas.

SUMMARY POINTS

1. CO_2 can be safely stored in the supercritical, or liquid-like, state in large porous structures within the Earth.
2. The rate of propagation is determined by the properties of the fluids and the porosity and permeability structure of the reservoir, and it can be influenced by the topography of confining boundaries.
3. Leakage rates are determined by the properties of the fluids and reservoir and by the geometry of injection and of the leakage pathway.
4. Surface tension effects between the CO_2 and intruded brine can be significant in changing the shape of the intruding CO_2 and also the amount trapped in the pore space.
5. The dissolution of CO_2 in brine leads to dense CO_2-saturated brine, which can convect downward, thereby stably storing dissolved CO_2.
6. The injection of CO_2 may cause measureable uplift and carries the risk of induced seismicity. These geomechanical effects need further consideration.

FUTURE ISSUES

1. How can researchers conduct a worthwhile, large-scale, field experiment to compare the field data with theoretical and laboratory models?
2. What is the fate of CO_2 leaked from the aquifer, and at what rate may it escape?
3. What is the displacement in the far field of brine due to the input of CO_2, and what are the implications for adjacent aquifers?
4. How best can the number of current injection sites be increased to accommodate the anthropogenic input of CO_2?
5. Is there a risk of induced seismicity, and if so, can it be mitigated?

DISCLOSURE STATEMENT

The authors are not aware of any biases that might be perceived as affecting the objectivity of this review.

ACKNOWLEDGMENTS

The authors acknowledge their many coauthors and colleagues who have provided and provoked many insights into the fluid mechanics of carbon sequestration. J.A.N. acknowledges funding from a Royal Society University Research Fellowship.

LITERATURE CITED

Acton JM, Huppert HE, Worster MG. 2001. Two-dimensional viscous gravity currents flowing over a deep porous medium. *J. Fluid Mech.* 440:359–80

Backhaus S, Turitsyn K, Ecke RE. 2011. Convective instability and mass transport of diffusion layers in a Hele-Shaw geometry. *Phys. Rev. Lett.* 106:104501
Bear J. 1972. *Dynamics of Fluids in Porous Media*. New York: Dover
Bickle MJ. 2009. Geological carbon storage. *Nat. Geosci.* 2:815–18
Bickle M, Chadwick A, Huppert HE, Hallworth MA, Lyle S. 2007. Modelling carbon dioxide accumulation at Sleipner: implications for underground carbon storage. *Earth Planet. Sci. Lett.* 255:164–76
Boait FC, White NJ, Bickle MJ, Chadwick RA, Neufeld JA, Huppert HE. 2012. Spatial and temporal evolution of injected CO_2 at the Sleipner Field, North Sea. *J. Geophys. Res.* 117:B03309
Elder JW. 1967. Steady free convection in a porous medium heated from below. *J. Fluid Mech.* 27:29–48
Ennis-King J, Paterson L. 2005. Role of convective mixing in the long-term storage of carbon dioxide in deep saline formations. *SPE J.* 10:349–56
Gasda SE, Nordbotten JM, Celia MA. 2009. Vertical equilibrium with sub-scale analytical methods for geological CO_2 sequestration. *Comput. Geosci.* 13:469–81
Golding MJ, Huppert HE. 2010. The effect of confining impermeable boundaries on gravity currents in a porous medium. *J. Fluid Mech.* 649:1–17
Golding MJ, Huppert HE, Neufeld JA. 2013. The effects of capillary forces on the axisymmetric propagation of two-phase, constant-flux gravity currents in porous media. *Phys. Fluids* 25:036602
Golding MJ, Neufeld JA, Hesse MA, Huppert HE. 2011. Two-phase gravity currents in porous media. *J. Fluid Mech.* 678:248–70
Graham MD, Steen PH. 1994. Plume formation and resonant bifurcations in porous-media convection. *J. Fluid Mech.* 272:67–89
Hesse MA, Orr FM Jr, Tchelepi HA. 2008. Gravity currents with residual trapping. *J. Fluid Mech.* 611:35–60
Hesse MA, Tchelepi HA, Cantwell J, Orr FM Jr. 2007. Gravity currents in horizontal porous layers: transition from early to late self-similarity. *J. Fluid Mech.* 577:363–83
Hewitt DR, Neufeld JA, Lister JR. 2012. Ultimate regime of high Rayleigh number convection in a porous medium. *Phys. Rev. Lett.* 108:224503
Hewitt DR, Neufeld JA, Lister JR. 2013. Convective shutdown in a porous medium at high Rayleigh number. *J. Fluid Mech.* 719:551–86
Howard LN. 1964. Convection at high Rayleigh number. *Proc. 11th Int. Cong. Appl. Mech.*, ed. H Görtler, pp. 1109–15. Berlin: Springer-Verlag
Huppert HE, Woods AW. 1995. Gravity-driven flows in porous layers. *J. Fluid Mech.* 292:55–69
Kochina IN, Mikhailov NN, Filinov MV. 1983. Groundwater mound damping. *Int. J. Eng. Sci.* 21:413–21
Lapwood ER. 1948. Convection of a fluid in a porous medium. *Math. Proc. Camb. Philos. Soc.* 44:508–21
Lüthi D, Le Floch M, Bereiter B, Blunier T, Barnola J-M, et al. 2008. High-resolution carbon dioxide concentration record 650,000–800,000 years before present. *Nature* 453:379–82
Lyle S, Huppert HE, Hallworth MA, Bickle M, Chadwick A. 2005. Axisymmetric gravity currents in a porous medium. *J. Fluid Mech.* 543:293–302
MacMinn CW, Juanes R. 2013. Buoyant currents arrested by convective dissolution. *Geophys. Res. Lett.* 40:2017–22
MacMinn CW, Neufeld JA, Hesse MA, Huppert HE. 2012. Spreading and convective dissolution of carbon dioxide in vertically confined, horizontal aquifers. *Water Resour. Res.* 48:W11516
Neufeld JA, Hesse MA, Riaz A, Hallworth MA, Tchelepi HA, Huppert HE. 2010. Convective dissolution of carbon dioxide in saline aquifers. *Geophys. Res. Lett.* 37:L22404
Neufeld JA, Huppert HE. 2009. Modelling carbon dioxide sequestration in layered strata. *J. Fluid Mech.* 625:353–70
Neufeld JA, Vella D, Huppert HE. 2009. The effect of a fissure on storage in a porous medium. *J. Fluid Mech.* 639:239–59
Neufeld JA, Vella D, Huppert HE, Lister JR. 2011. Leakage from gravity currents in a porous medium. Part 1. A localised sink. *J. Fluid Mech.* 666:391–413
Nield DA, Bejan A. 2006. *Convection in Porous Media*. New York: Springer
Nordbotten JA, Celia MA. 2006. Similarity solutions for fluid injection into confined aquifers. *J. Fluid Mech.* 561:307–27

Nordbotten JA, Celia MA, Bachu S, Dahle H. 2005. Semianalytical solution for CO_2 leakage through an abandoned well. *Environ. Sci. Technol.* 39:602–11

Otero J, Dontcheva LA, Johnston H, Worthing RA, Kurganov A, et al. 2004. High-Rayleigh-number convection in a fluid-saturated porous layer. *J. Fluid Mech.* 500:263–81

Pau GSH, Bell JB, Pruess K, Almgren AS, Lijewski MJ, Zhang K. 2010. High-resolution simulation and characterization of density-driven flow in CO_2 storage in saline aquifers. *Adv. Water Resour.* 33:443–55

Pegler SS, Huppert HE, Neufeld JA. 2013. Topographic controls on gravity currents in porous media. *J. Fluid Mech.* Manuscript under review

Phillips OM. 1991. *Geological Fluid Dynamics: Sub-Surface Flow and Reactions.* Cambridge, UK: Cambridge Univ. Press

Pritchard D. 2007. Gravity currents over fractured substrates in a porous medium. *J. Fluid Mech.* 584:415–31

Pritchard D, Woods AW, Hogg AJ. 2001. On the slow draining of a gravity current moving through a layered permeable medium. *J. Fluid Mech.* 444:23–47

Riaz A, Hesse M, Tchelepi HA, Orr FM Jr. 2006. Onset of convection in a gravitationally unstable diffusive boundary layer in porous media. *J. Fluid Mech.* 548:87–111

Rucci A, Vasco DW, Novali F. 2013. Monitoring the geologic storage of carbon dioxide using multicomponent SAR interferometry. *Geophys. J. Int.* 193:197–208

Shepherd J, Caldeira K, Cox P, Haigh J, Keith D, et al. 2009. Geoengineering the climate: science, governance and uncertainty. *Rep*, R. Soc. London

Slim AC, Ramakrishnan TS. 2010. Onset and cessation of time-dependent, dissolution-driven convection in porous media. *Phys. Fluids* 22:124103

Stevens JD, Sharp JM Jr, Simmons CT, Fenstemaker TR. 2009. Evidence of free convection in groundwater: field-based measurements beneath wind-tidal flats. *J. Hydrol.* 375:394–409

Vella D, Huppert HE. 2006. Gravity current in a porous medium in an inclined plane. *J. Fluid Mech.* 555:353–62

Vella D, Neufeld JA, Huppert HE, Lister JR. 2011. Leakage from gravity currents in a porous medium. Part 2. A line sink. *J. Fluid Mech.* 666:414–27

White DJ, Burrowes G, Davis T, Hajnal Z, Hirsche K, et al. 2004. Greenhouse gas sequestration in abandoned oil reservoirs: the International Energy Agency Weyburn pilot project. *GSA Today* 14:4–10

Woods AW, Farcas A. 2009. Capillary entry pressure and the leakage of gravity currents through a sloping layered permeable rock. *J. Fluid Mech.* 618:361–79

Zimoch PJ, Neufeld JA, Vella D. 2011. Leakage from inclined porous reservoirs. *J. Fluid Mech.* 673:395–405

Zoback MD, Gorelick SM. 2013. Earthquake triggering and large-scale geologic storage of carbon dioxide. *Proc. Natl. Acad. Sci. USA.* In press

Annual Review of
Fluid Mechanics

Volume 46, 2014

Contents

Indexes

Errata

An online log of corrections to *Annual Review of Fluid Mechanics* articles may be found at http://fluid.annualreviews.org/errata.shtml